

1 **Direct probing of acylperoxy radicals during ozonolysis of α -pinene: constraints on**
2 **radical chemistry and production of highly oxygenated organic molecules**

3 Han Zang¹, Dandan Huang², Jiali Zhong³, Ziyue Li¹, Chenxi Li¹, Huayun Xiao¹, Yue Zhao^{1,*}

4

5 ¹School of Environmental Science and Engineering, Shanghai Jiao Tong University, Shanghai,
6 200240, China

7 ²Shanghai Academy of Environmental Sciences, Shanghai 200233, China

8 ³Division of Environment and Sustainability, Hong Kong University of Science and Technology,
9 Hong Kong SAR, 999077, China

10

11 *Correspondence: Yue Zhao (yuezhao20@sjtu.edu.cn)

12

13 **Abstract**

14 Acylperoxy radicals (RO₂) are key intermediates in atmospheric oxidation of organic compounds
15 and different from the general alkyl RO₂ radicals in reactivity. However, direct probing of the
16 molecular identities and chemistry of acyl RO₂ remains quite limited. Here, we report a combined
17 experimental and kinetic modelling study of the composition and formation mechanisms of acyl
18 RO₂, as well as their contributions to the formation of highly oxygenated organic molecules (HOMs)
19 during ozonolysis of α -pinene. We find that acyl RO₂ radicals account for 67%, 94%, and 32% of
20 the highly oxygenated C₇, C₈, and C₉ RO₂, respectively, but only a few percent of C₁₀ RO₂. The
21 formation pathway of acyl RO₂ species depends on their oxygenation level. The highly oxygenated
22 acyl RO₂ (oxygen atom number ≥ 6) are mainly formed by the intramolecular aldehydic H-shift (i.e.,
23 autoxidation) of RO₂, while the less oxygenated acyl RO₂ (oxygen atom number < 6) are basically
24 derived from the C-C bond cleavage of alkoxy (RO) radicals containing an α -ketone group or the
25 intramolecular H-shift of RO containing an aldehyde group. The acyl RO₂-involved reactions
26 explain 50-90% of C₇ and C₈ closed-shell HOMs and 14% of C₁₀ HOMs, respectively. For C₉ HOMs,
27 this contribution can be up to 30%-60%. In addition, acyl RO₂ contribute to 50%-95% of C₁₄-C₁₈
28 HOM dimer formation. Because of the generally fast reaction kinetics of acyl RO₂, the acyl RO₂ +
29 alkyl RO₂ reactions seem to outcompete the alkyl RO₂ + alkyl RO₂ pathways, thereby affecting the
30 fate of alkyl RO₂ and HOM formation. Our study sheds lights on the detailed formation pathways
31 of the monoterpene-derived acyl RO₂ and their contributions to HOM formation, which will help to
32 understand the oxidation chemistry of monoterpenes and sources of low-volatility organic
33 compounds capable of driving particle formation and growth in the atmosphere.

34 1. Introduction

35 Monoterpenes ($C_{10}H_{16}$) comprise an important fraction of nonmethane hydrocarbons in the global
36 atmosphere (Guenther et al., 2012; Sindelarova et al., 2014) and make a significant contribution to
37 the secondary organic aerosol (SOA) budget (Pye et al., 2010; Iyer et al., 2021). The presence of
38 double bond and large molecular size of monoterpenes favor their oxidation reactivity towards O_3 ,
39 hydroxyl (OH), and nitrate (NO_3) radicals (Atkinson et al., 1990; Roger et al., 2004; Kurten et al.,
40 2015; Kristensen et al., 2016; Bianchi et al., 2019; Berndt, 2022), as well as the formation of low-
41 volatility products and SOA (Fry et al., 2009; Fry et al., 2014; Zhang et al., 2018; Bianchi et al.,
42 2019; Molteni et al., 2019; Shen et al., 2022). The organic peroxy radicals (RO_2) in the gas-phase
43 oxidation of monoterpenes can undergo autoxidation and form a class of highly oxygenated organic
44 compounds (HOM) (Jokinen et al., 2014; Mentel et al., 2015; Berndt et al., 2016; Zhao et al., 2018;
45 Bianchi et al., 2019; Bell et al., 2021; Berndt, 2022), which are primarily low- or extremely low-
46 volatility organic compounds (LVOCs and ELVOCs) (Ehn et al., 2014; Bianchi et al., 2019) and
47 thus play a crucial role in SOA formation and growth.

48 Significant advances have been made in recent years concerning the monoterpene RO_2 autoxidation
49 and its contribution to HOM formation (Ehn et al., 2014; Berndt et al., 2016; Zhao et al., 2018; Xu
50 et al., 2019; Lin et al., 2021; Berndt, 2022; Shen et al., 2022). It is recognized that a part of
51 monoterpene RO_2 radicals derived from the traditional ozonolysis channel (i.e., isomerization of
52 Criegee intermediates, CI) and OH addition channel can autoxidize at a rate larger than 1 s^{-1} and
53 could be an important contributor to HOM formation (Zhao et al., 2018; Xu et al., 2019; Berndt,
54 2021). Recently, new reaction channels leading to the RO_2 radicals that can undergo fast
55 autoxidation have been proposed. A quantum chemical calculation study indicated that an excited
56 CI arising from α -pinene ozonolysis could undergo ring-breaking reactions and directly lead to a
57 ring-opened RO_2 due to the excess energy, which can autoxidize at a rate of $\sim 1\text{ s}^{-1}$ and rapidly form
58 highly oxidized RO_2 with up to 8 oxygen atoms (Iyer et al., 2021). In addition, the minor hydrogen
59 abstraction channel by OH radicals has been proposed as a predominant pathway to HOM formation
60 from OH oxidation of α -pinene under atmospheric conditions (Shen et al., 2022).

61 RO_2 species can be simply divided into alkyl RO_2 and acyl RO_2 ($RC(O)OO$) according to whether
62 R is an acyl radical. There are significant differences in the reactivity of these two kinds of RO_2 .
63 Firstly, the rate constant of acyl RO_2 with NO is in general slightly higher than that of alkyl RO_2
64 (Atkinson et al., 2007; Calvert et al., 2008; Orlando and Tyndall, 2012). For example, the reaction
65 rate constants of acyl RO_2 , $CH_3C(O)O_2$, and alkyl RO_2 , $CH_3CH_2O_2$, with NO have been reported to
66 be $20 \times 10^{-12}\text{ cm}^3\text{ molecule}^{-1}\text{ s}^{-1}$ and $9.2 \times 10^{-12}\text{ cm}^3\text{ molecule}^{-1}\text{ s}^{-1}$, respectively (Atkinson et al., 2007;

67 Calvert et al., 2008; Orlando and Tyndall, 2012). Besides, acyl RO₂ can react rapidly with NO₂ and
68 form thermally unstable peroxyacyl nitrates (RC(O)OONO₂), which have a lifetime of tens of
69 minutes at room temperature and of days and even months in winter or in the upper atmosphere with
70 lower temperatures (Atkinson et al., 2007; Orlando and Tyndall, 2012). Although alkyl RO₂ radicals
71 can also react with NO₂ and form the alkyl peroxy nitrates (ROONO₂), they are extremely unstable
72 and will decompose into RO₂ radicals and NO₂ in less than 1s (Kirchner et al., 1997; Orlando and
73 Tyndall, 2012). Lastly, the rate constant of cross-reaction of acyl RO₂ ($1.5 \pm 0.3 \times 10^{-11} \text{ cm}^3$
74 $\text{molecule}^{-1} \text{ s}^{-1}$) is significantly higher than that of alkyl RO₂ ($2 \times 10^{-17} - 1 \times 10^{-11} \text{ cm}^3 \text{ molecule}^{-1} \text{ s}^{-1}$)
75 (Villenave and Lesclaux, 1996; Tyndall et al., 2001; Atkinson et al., 2007; Zhao et al., 2018). As a
76 result, these two kinds of RO₂ may play different roles in the autoxidation as well as HOM and
77 dimer formation.

78 The quantum calculations revealed that different functional groups in RO₂ would lead to
79 significantly different intramolecular H-shift rates (Otkjær et al., 2018). The C=O and C=C
80 substituents lead to resonance stabilized carbon radicals and could enhance the H-shift rate constants
81 by more than a factor of 400. The fast aldehydic H-shift rate contributes to a series of acyl radicals
82 (RC(O)) with the radical site at the terminal carbonyl carbon, which further produce the acyl RO₂
83 with O₂ addition. Many RO₂ formed in the oxidation of monoterpenes have the aldehyde
84 functionality, especially for α -pinene ozonolysis, in which all the primary and many later-generation
85 RO₂ contain at least one aldehyde group (Noziere et al., 2015; Berndt et al., 2018; Li et al., 2019;
86 Berndt, 2022; Zhao et al., 2022). As a result, acyl RO₂ may comprise a considerable fraction of total
87 RO₂ species and contribute significantly to the formation of low-volatility products and SOA in the
88 monoterpene oxidation system. A recent study by Zhao et al. (2022) found that the acyl RO₂-
89 involved reactions contribute to 50%-80% of oxygenated C₁₅-C₂₀ dimers (O:C \geq 0.4) and 70% of
90 C₁₅-C₁₉ dimer esters in SOA from α -pinene ozonolysis. However, currently the direct probing of
91 the molecular identities and chemistry of monoterpene-derived acyl RO₂ radicals is rather limited.
92 The role of acyl RO₂ in HOM formation remains to be quantified.

93 In this study, the molecular identities and formation mechanisms of acyl RO₂ radicals, as well as
94 their contributions to HOM formation in the α -pinene ozonolysis are investigated. The experiments
95 were conducted in a flow reactor with different concentrations of NO₂, which acted as an efficient
96 scavenger for the acyl RO₂. The molecular composition and abundance of the gas-phase HOMs
97 were measured by a chemical ionization-atmospheric pressure interface-time-of-flight mass
98 spectrometer (CI-API-TOF) using nitrate as the reagent ions. In addition, kinetic modelling using
99 the Framework for 0-D Atmospheric Modeling (F0AM v4.1) employing Master Chemical

100 Mechanisms (MCM v3.3.1) updated with the latest advances of the RO₂ chemistry was performed
101 to gain insights into the reaction kinetics and mechanisms of acyl RO₂ species. We find that acyl
102 RO₂ account for a major fraction of highly oxygenated C₇ and C₈ RO₂ and play a significant role in
103 the formation of HOM monomers and dimers with small molecular size. This study will help to
104 understand the role of acyl RO₂ in the formation of low-volatility species from monoterpene
105 oxidation and reduce the uncertainties in the future atmospheric modelling of the formation and
106 impacts of aerosols.

107 **2. Method and Materials**

108 **2.1 Flow Reactor Experiments.**

109 The α -pinene ozonolysis experiments were carried out under room temperature (298 K) and dry
110 conditions (relative humidity < 5%) in a custom-built flow reactor, which has been described in detail
111 previously (Yao et al., 2019). The α -pinene vapor was generated by evaporating its pure liquid (99%,
112 Sigma-Aldrich) into a flow of zero air (10.65 L min⁻¹) added to the reactor using an automated
113 syringe pump (TYD01-01-CE, Baoding Leifu Fluid Technology Co., Ltd.). The initial
114 concentrations of α -pinene ranged from 500 ppb to 3 ppm in different experiments. Ozone was
115 generated by passing a flow of ultra-high-purity (UHP) O₂ (150 mL min⁻¹, Shanghai Maytor Special
116 Gas Co., Ltd.) through a quartz tube housing a pen-ray mercury lamp (UV-S2, UVP Inc.) and its
117 concentration (45 ppb and 180 ppb under low and high O₃ conditions, respectively) was measured
118 by an ozone analyzer (Model 49i, Thermo Fisher Scientific, USA). The NO₂, acting as an acyl RO₂
119 scavenger, was derived from its standard cylinder gas (15.6 ppm, Shanghai Weichuang Standard
120 Gas Co., Ltd.) and its initial concentration ranged from 0 to 30 ppb. To validate the formation
121 mechanisms of acyl RO₂, selected experiments with the addition of NO or cyclohexane were also
122 conducted. NO was derived by its standard cylinder gas (9.8 ppm, Shanghai Weichuang Standard
123 Gas Co., Ltd.) and its initial concentration also ranged from 0 to 30 ppb. The gas-phase cyclohexane
124 (~ 500 ppm), acting as an OH scavenger, was generated by bubbling a gentle flow of UHP N₂
125 through liquid cyclohexane (LC-MS grade, CNW). The total air flow in the flow reactor was 10.8 L
126 min⁻¹ and the residence time was 25 seconds. The relatively low O₃ concentration and short reaction
127 time in the flow reactor avoid significant production of NO₃ radicals from NO₂ and O₃ and make
128 the NO₃ oxidation contribute only 0.3%-1.2% of the total α -pinene oxidation in our experiments.
129 Therefore, the NO₃ chemistry could be neglected in this study. A summary of the experimental
130 conditions is given in Tables S1 and S2 in the Supplement.

131 The gas-phase RO₂ radicals and closed-shell products were measured by a nitrate-based CI-API-
132 TOF mass spectrometer (abbreviated as nitrate-CIMS; Aerodyne Research, Inc.), and a long time-

133 of-flight mass spectrometer with a mass resolution of ~ 10000 Th/Th was used here. The mass
134 calibration error is below 1.8 ppm. The sheath flow, including a 2 mL min^{-1} UHP N_2 flow containing
135 nitric acid (HNO_3) and 22.4 L min^{-1} zero air was guided through a PhotoIonizer X-ray (Model L9491,
136 Hamamatsu, Japan) to generate nitrate reagent ions. The total sample flow rate was 9 L min^{-1} during
137 the experiments. The mass spectra within the m/z range of 50 to 700 were analyzed using the
138 tofTools package developed by Junninen et al. (2010) based on Matlab.

139 To clarify whether there is SOA formation in the experiments, a scanning mobility particle sizer
140 (SMPS, TSI), which consists of an electrostatic classifier (model 3082), a long or nano differential
141 mobility analyzer (model 3081 and 3085 for different particle sizes), and a condensation particle
142 counter (model 3756), was used to monitor the formation of SOA particles. Except in Exp 31 where
143 the reacted α -pinene reached 36.8 ppb and there was low SOA formation with particle mass
144 concentrations of 5.0×10^{-4} - $5.7 \times 10^{-3} \mu\text{g m}^{-3}$ and number concentrations of 63 - 395 cm^{-3} , no particle
145 formation was observed by SMPS. Therefore, the RO_2 radicals and closed-shell products would be
146 primarily distributed in the gas phase, with their fates negligibly influenced by the low SOA
147 formation under these experimental conditions.

148 **2.2 Kinetic Model Simulations.**

149 Model simulations of RO_2 and HOM formation in selected experiments were performed to constrain
150 the reaction kinetics and mechanisms of acyl RO_2 using FOAM v4.1 (Wolfe et al., 2016), which
151 employs MCM v3.3.1 (Jenkin et al., 2015) updated with the chemistry of RO_2 autoxidation and
152 cross-reactions forming HOM monomers and dimers. Newly added species and reactions to MCM
153 v3.3.1 followed the work by Zhao et al. (2018) and Wang et al. (2021). Considering that the default
154 MCM v3.3.1 does not include highly oxygenated acyl RO_2 , we added the possible formation
155 pathways of the potential acyl RO_2 measured in this study to the model based on the mechanisms
156 proposed by Zhao et al. (2022).

157 The formation and reaction branching ratios of the two α -pinene-derived CIs are updated in the
158 model according to the recent studies (Table S3) (Claflin et al., 2018; Iyer et al., 2021; Zhao et al.,
159 2021; Berndt, 2022). The formation of a ring-opened $\text{C}_{10}\text{H}_{15}\text{O}_4\text{-RO}_2$ species (C10H15O4RBRO2 in
160 Table S3) from α -pinene ozonolysis proposed by a recent study (Iyer et al., 2021), as well as its
161 subsequent autoxidation and bimolecular reactions, is included in the model. The autoxidation rate
162 constant of the ring-opened $\text{C}_{10}\text{H}_{15}\text{O}_4\text{-RO}_2$ is 1 s^{-1} , and a lower limit of its molar yield (30%) was
163 used according to the recent studies (Zhao et al., 2021; Meder et al., 2023) and our results (see
164 details in Section 3.3). We also added the hydrogen abstraction channel of α -pinene oxidation by
165 OH radicals according to a recent study (Shen et al., 2022). The branching ratio of this channel was

166 set to 9%, with the rest 91% being the traditional OH addition pathways. The detailed reaction
167 pathways and rate constants of RO₂ species in this channel followed the work by Shen et al. (2022),
168 except for RO₂ cross-reactions, the rates of which were not reported in that study. As the primary
169 RO₂ radicals (C₁₀H₁₅O₂-RO₂) formed via the hydrogen abstraction by OH radical are least-oxidized
170 with only 2 oxygen atoms, their cross-reaction rate could be relatively low (Atkinson et al., 2007;
171 Orlando and Tyndall, 2012). In the model, this rate constant was set to $1 \times 10^{-13} \text{ cm}^3 \text{ molecule}^{-1} \text{ s}^{-1}$.
172 For other alkyl RO₂ radicals (including HOM-RO₂), their cross-reaction rate constant is assumed to
173 be $1 \times 10^{-12} \text{ cm}^3 \text{ molecule}^{-1} \text{ s}^{-1}$ according to Zhao et al. (2018). The dimer formation rates for these
174 alkyl RO₂ are same as their cross-reaction rates.

175 In flow reactor experiments, the equilibrium formation of ROONO₂ would lead to the consumption
176 of alkyl RO₂ radicals. To account for the influence of this process on the RO₂ budget and HOM
177 formation, we included the reaction of $\text{RO}_2 + \text{NO}_2 \rightleftharpoons \text{ROONO}_2$ in the model, with forward and
178 reverse reaction rate constants of $7.5 \times 10^{-12} \text{ cm}^3 \text{ molecule}^{-1} \text{ s}^{-1}$ and 5 s^{-1} , respectively (Orlando and
179 Tyndall, 2012). To simplify the parameterization, the forward and reverse reaction rate constants of
180 newly added highly oxygenated acyl RO₂ with NO₂ are the same as default values in MCM v3.3.1.
181 Besides, the cross-reaction rate constants of acyl RO₂ (including acyl RO₂ + acyl RO₂ and acyl RO₂
182 + alkyl RO₂) forming monomers or dimers were both set to $1 \times 10^{-11} \text{ cm}^3 \text{ molecule}^{-1} \text{ s}^{-1}$ (Orlando
183 and Tyndall, 2012). Considering that there are large uncertainties in the dimer formation rate of RO₂,
184 a sensitivity analysis was conducted to evaluate its influence on acyl RO₂-involved HOM formation
185 by varying the rate constant from $1 \times 10^{-13} \text{ cm}^3 \text{ molecule}^{-1} \text{ s}^{-1}$ to $1 \times 10^{-12} \text{ cm}^3 \text{ molecule}^{-1} \text{ s}^{-1}$ for alkyl
186 RO₂ and $1 \times 10^{-12} \text{ cm}^3 \text{ molecule}^{-1} \text{ s}^{-1}$ to $1 \times 10^{-11} \text{ cm}^3 \text{ molecule}^{-1} \text{ s}^{-1}$ for acyl RO₂. The results show
187 that changes in dimer formation rate constants within the above ranges have no significant influence
188 on the contribution of acyl RO₂ to HOM formation (Figure S1).

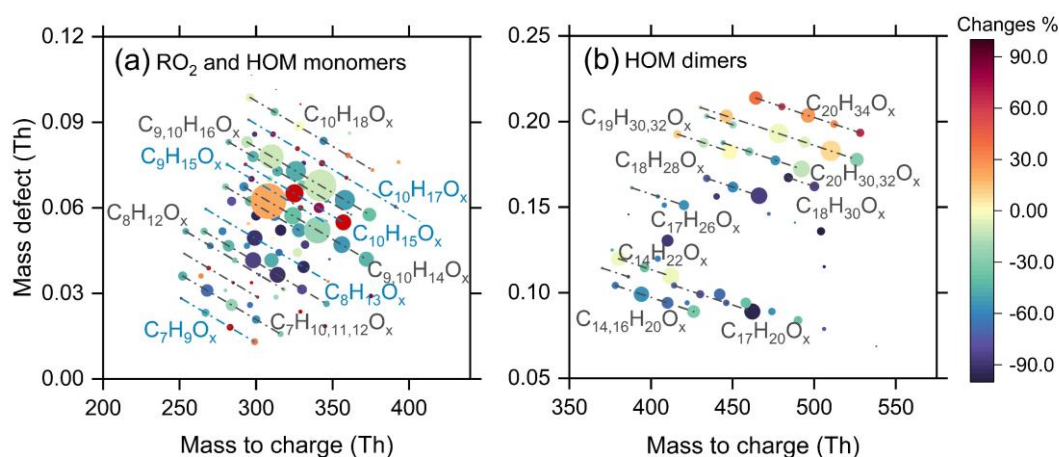
189 The wall losses of OH, HO₂, and RO₂ radicals, as well as closed-shell HOM monomers and dimers
190 in the flow reactor were considered using the KPS method proposed by Knopf et al. (2015) in the
191 model (Table S4), with an assumption of irreversible uptake of these species on the reactor wall. It
192 is found that the wall loss of OH, HO₂, and RO₂ radicals accounts for 0.08-0.14%, 4.7-9.1%, and 7.3-
193 25.5% of their total production, respectively, with lower values under higher reacted α -pinene
194 concentration conditions. Therefore, the wall loss process would not significantly influence α -
195 pinene oxidation and RO₂ chemistry. The wall losses of closed-shell HOM monomers and dimers
196 account for 18.4-34.7% and 14.2-33.1% of their total production, respectively. It should be noted
197 that the wall losses of typical RO₂ and HOMs have negligible impact on their responses to the
198 addition of NO₂ (Figure S2). In addition, with the consideration of the wall loss effects, the effect

199 and contribution of acyl RO₂ to the HOM formation only changed a little (0.02-0.5%). Therefore,
200 the wall losses of RO₂ and HOMs in the flow reactor would not affect the interpretation of the results
201 in this study.

202 3. Results and Discussion

203 3.1 Molecular composition of acyl RO₂ from α -pinene ozonolysis

204 The overall formation characteristics of gas-phase RO₂, closed-shell monomers, and dimers with
205 the addition of NO₂ (30 ppb) is shown in Figure 1 (Exps 8 and 14, Table S1). Since nitrate-CIMS is
206 only highly sensitive to the highly oxygenated species, we only discuss the production of HOMs
207 with oxygen atoms above 6 here. As for RO₂ and closed-shell monomers (Figure 1a), the signals of
208 C₇ and C₈ species decrease by more than 50% with the addition of NO₂, while for C₉ and C₁₀ species,
209 their decreases are relatively small (within 40%). In addition, we note that there is an unexpected
210 increase in some C₉ and C₁₀ RO₂, and the possible reason will be discussed in detail later.

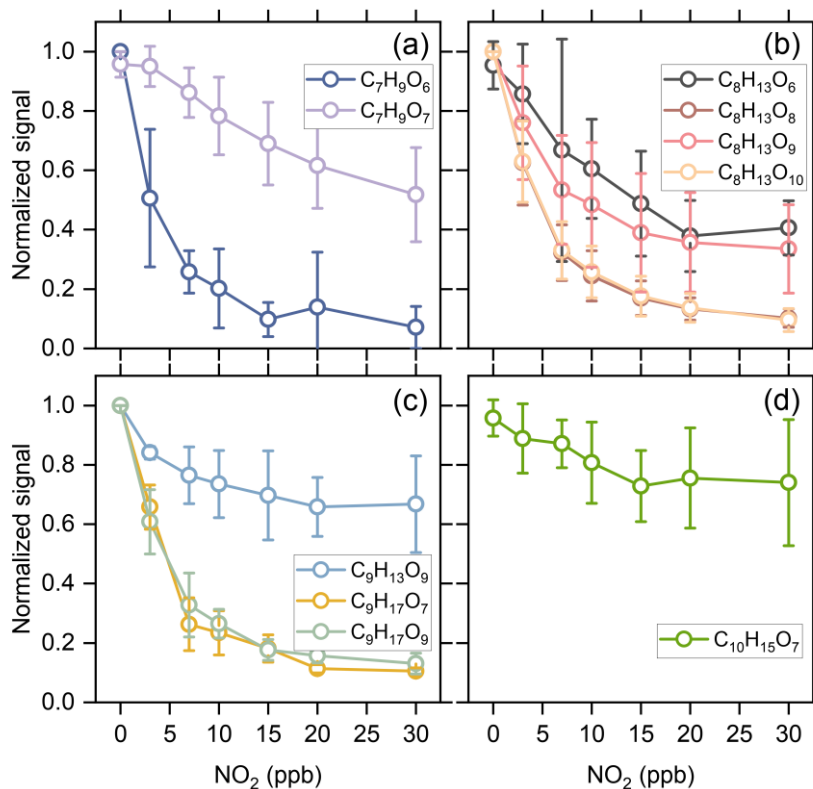


211
212 Figure 1 Mass defect plots of (a) RO₂, HOM monomers, and (b) HOM dimers formed from
213 ozonolysis of α -pinene in the presence of NO₂ measured using nitrate-CIMS (Exps 8, 14). The
214 circles are colored by the relative changes in signal of RO₂, monomers and dimers due to the addition
215 of NO₂ (30 ppb). The area of circles is linearly scaled with the cube root of the signal of HOMs
216 formed in the absence of NO₂. The blue lines represent RO₂ radicals.

217 NO₂ could react rapidly with acyl RO₂ radicals to form RC(O)OONO₂, which has a higher thermal-
218 stability compared to ROONO₂ and can serve as a sink for acyl RO₂ on our experimental timescales.
219 Therefore, a significant decrease in C₇ and C₈ RO₂ and HOMs upon the addition of NO₂ indicates
220 that a major fraction of C₇ and C₈ RO₂ are acyl RO₂. In contrast, the slight decrease in C₉ and C₁₀
221 HOM monomers shows that the contribution of acyl RO₂ to C₉ and C₁₀ RO₂ is relatively small.
222 However, some of the C₁₀ monomers showed a slight increase with the addition of NO₂, especially

223 for $C_{10}H_{18}O_x$ -HOMs. The addition of NO_2 plays a twofold role in dimer formation from α -pinene
224 ozonolysis (Figure 1b). There is a significant inhibiting effect on C_{14} - C_{18} dimers, which is due to
225 the large contribution of acyl RO_2 to the total C_7 and C_8 RO_2 that generate such dimers. However,
226 C_{19} and C_{20} dimers only show a slight decrease with the addition of NO_2 , and some of them are even
227 enhanced. In particular, the enhancement in $C_{20}H_{34}O_x$ is most significant, reaching 30%.

228 Kinetic model simulations show that the concentration of alkyl RO_2 decreases by 1-20% with the
229 addition of 30 ppb NO_2 under different reacted α -pinene conditions (Exps 1-28). Considering that
230 the acyl RO_2 could be rapidly consumed by NO_2 , if the signal reduction of a RO_2 specie significantly
231 exceeds 20% with 30 ppb NO_2 addition, we presume it has significant contribution from acyl RO_2 .
232 As a result, a total of 10 acyl RO_2 were identified according to the changes of RO_2 signal as a
233 function of initial NO_2 concentration, which include $C_7H_9O_6$, $C_7H_9O_7$, $C_8H_{13}O_6$, $C_8H_{13}O_8$, $C_8H_{13}O_9$,
234 $C_8H_{13}O_{10}$, $C_9H_{13}O_9$, $C_9H_{17}O_7$, $C_9H_{17}O_9$, and $C_{10}H_{15}O_7$. Figure 2 shows the averaged normalized acyl
235 RO_2 signals measured as a function of the added NO_2 concentration under different experimental
236 conditions (Exps 1-28). Similarly, since nitrate-CIMS is only highly sensitive to products with high
237 oxygen content, we only observed acyl RO_2 with oxygen atoms above 6. Consistent with the
238 significant decrease in C_7 and C_8 species with the addition of NO_2 in Figure 1a, C_7 and C_8 acyl RO_2
239 decrease by more than 50% with the increase of NO_2 concentration (Figures 2a, b). For C_9 acyl RO_2 ,
240 the $C_9H_{17}O_7$ - RO_2 and $C_9H_{17}O_9$ - RO_2 also decrease dramatically with increasing NO_2 , and the
241 decrease in $C_9H_{13}O_9$ - RO_2 is relatively smaller (Figure 2c). In addition, $C_{10}H_{15}O_7$ - RO_2 also shows a
242 small decrease (Figure 2d), with a reduction of only 30% at 30 ppb NO_2 . The relatively small
243 reduction in the abundance of some of these RO_2 radicals indicates the presence of alkyl RO_2
244 radicals with the same chemical formulas. Along with the marked reduction in acyl RO_2 signals, the
245 production of highly oxygenated $RC(O)OONO_2$ species such as $C_9H_{13}O_9NO_2$, $C_9H_{17}O_7NO_2$, and
246 $C_{10}H_{15}O_7NO_2$ with the addition of NO_2 were observed (see the spectra in Figure S3). However, we
247 note that although some $RC(O)OONO_2$ such as $C_8H_{13}O_6NO_2$ and $C_8H_{13}O_8NO_2$ are expected to be
248 formed with NO_2 addition, they could not be unambiguously detected by nitrate-CIMS due to the
249 overlapping of their peaks with strong alkyl RO_2 peaks ($C_9H_{15}O_8$ - RO_2 and $C_9H_{15}O_{10}$ - RO_2) in this
250 study.

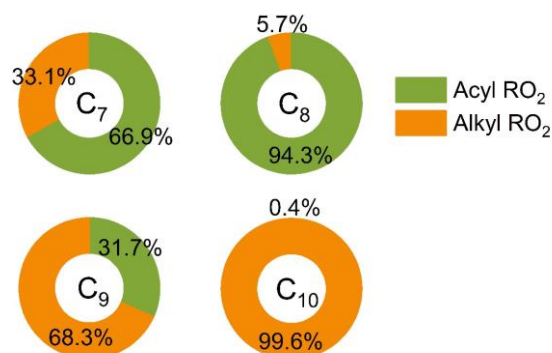


251

252 Figure 2 Averaged normalized signal of the measured acyl RO₂ as a function of the added NO₂
 253 concentration under different experimental conditions (Exps 1-28).

254 Figure 3 shows the contribution of acyl and alkyl RO₂ to the highly oxygenated C₇-C₁₀ RO₂. Acyl
 255 RO₂ contribute 66.9%, 94.3% and 31.7% to the total C₇, C₈, and C₉ RO₂ signals, respectively. By
 256 contrast, the only C₁₀ acyl RO₂ measured in this study is C₁₀H₁₅O₇, which contributes to only 0.4%
 257 of the total C₁₀ RO₂. It should be note that there might be other C₁₀ acyl RO₂ that were not observed
 258 due to the interferences from the alkyl RO₂ with the same chemical formulas, which respond
 259 differently to the addition of NO₂ than acyl RO₂ do (see details in the following discussion).
 260 Considering that some RO₂ formulas such as C₁₀H₁₅O₇ may have contributions from both acyl RO₂
 261 and alkyl RO₂, we assumed the decrease of RO₂ signal with the addition of NO₂ as the signal of acyl
 262 RO₂. Besides, it is obvious that the normalized signal basically decreases to the lowest value when
 263 the initial NO₂ concentration reaches 10 ppb (Figure 2), indicating that most of the acyl RO₂ are
 264 depleted at this NO₂ concentration. In addition, the decreasing extents of some acyl RO₂ are different
 265 for different reacted α -pinene concentrations, with lower decreasing extent for higher reacted α -
 266 pinene concentrations (Figure S4). This difference might be due to the promoted cross-reactions of
 267 acyl RO₂ as well as their precursor RO₂ at higher α -pinene concentrations, which are competitive
 268 with the reactions leading to acyl RO₂ formation as well as the acyl RO₂ + NO₂ reactions.

269



270
 271 Figure 3 Contributions of acyl and alkyl RO₂ to the highly oxygenated C₇-C₁₀ RO₂ measured by
 272 nitrate-CIMS.

273 In addition to the changes of acyl RO₂ signal, we also show the changes of normalized alkyl RO₂
 274 signal with the increasing initial NO₂ concentration in Figure S5. Although ROONO₂ formed by the
 275 reaction of alkyl RO₂ with NO₂ is thermally unstable and would decompose quickly to release RO₂,
 276 it would still reach a formation/decomposition equilibrium in the system, thus consuming a small
 277 amount of alkyl RO₂. However, it can be seen from Figure S5 that during 25 s of reaction in the
 278 flow reactor, a large part of alkyl RO₂ has an increasing trend with the increase of NO₂ concentration.
 279 We speculate that a portion of ROONO₂ could decompose back to RO₂ and NO₂ in the nitrate
 280 chemical ionization inlet where the sample gases were diluted instantly and the equilibrium of
 281 ROONO₂ was disturbed, resulting in the release of a large amount of RO₂.

282

283 To verify our speculation, the decomposition of ROONO₂ in the chemical ionization inlet was
 284 simulated based on the dilution ratio (1:3.5) and residence time (200 ms) in the inlet. As shown in
 285 Figure S6, more than 40% of ROONO₂ decompose back to RO₂ and NO₂ in the chemical ionization
 286 inlet, which would inevitably lead to an increase in RO₂ concentration. As the C₁₀H₁₅O₈NO₂ has a
 287 significant contribution from the relative stable RC(O)OONO₂ arising from the ring-opened acyl
 288 C₁₀H₁₅O₈-RO₂ reported by Iyer et al. (2021), its decomposition is relatively small (~21%). It should
 289 be noted that the RO₂ measured here is only a part of total RO₂ and that a large amount of RO₂ has
 290 already reacted to form closed-shell products as well as ROONO₂ in the flow reactor. Taking Exp
 291 14 as an example (30 ppb NO₂), the simulated concentrations of RO₂ and ROONO₂ are 1.3 ppb and
 292 1.9 ppb, which approximately accounts for 27.1% and 39.6% of the total production of RO₂,
 293 respectively. Therefore, the decomposition of ROONO₂ could indeed result in an increase in the
 294 RO₂ signal. It should also be pointed out that because of the very short residence time in the chemical
 295 ionization inlet, such an increase in the RO₂ concentration would not significantly impact HOM
 296 formation.

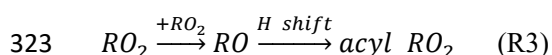
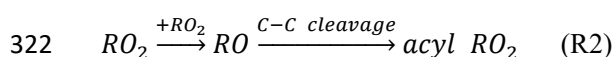
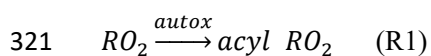
297 To confirm the reliability of our results, we examined the changes in the signals of RO₂ and closed-
 298 shell products as a function of reacted α -pinene in the absence of NO₂ (Section S1 and Figure S7),

299 and the results are consistent with previous studies (Zhao et al., 2018). In addition, we repeated Exps
300 15-21 on another nitrate-CIMS and a similar increase in alkyl RO₂ signals with the addition of NO₂
301 was observed on that instrument (Figure S8).

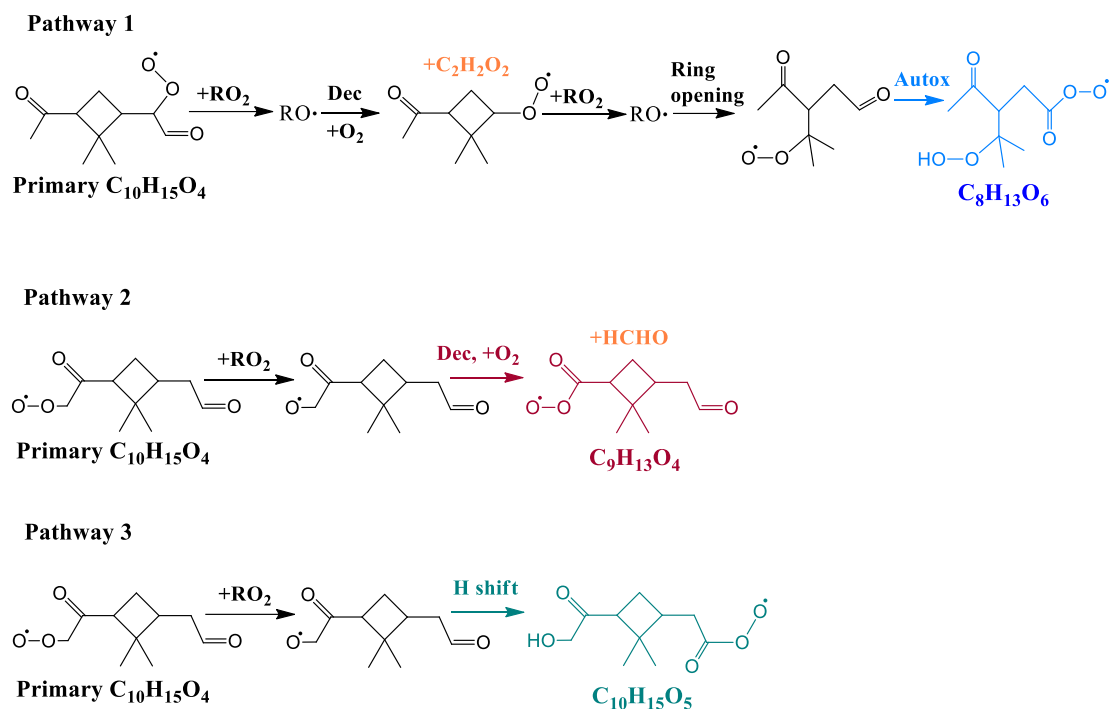
302 3.2 Formation mechanisms of acyl RO₂ during α -pinene ozonolysis

303 It has been recently suggested that there are three main pathways that directly lead to the formation
304 of monoterpene-derived acyl RO₂ (Zhao et al., 2022): (i) the autoxidation of RO₂ containing
305 aldehyde groups (Reaction R1), (ii) the cleavage of C-C bond of RO containing an α -ketone group
306 (Reaction R2), and (iii) the intramolecular H-shift of RO containing an aldehyde group (Reaction
307 R3). In addition, the secondary OH oxidation of aldehyde products can also produce acyl RO₂
308 radicals. However, in the present study, the secondary OH oxidation is expected to be insignificant
309 due to an excess of α -pinene compared to O₃. Indeed, kinetic model simulations incorporating the
310 secondary OH chemistry show that the contribution of secondary OH oxidation to acyl RO₂
311 formation is negligible even under high O₃ conditions (see details in Section S2 and Figure S9).

312 Here, we further investigated the formation mechanisms of acyl RO₂. Figure 4 shows the reaction
313 schemes leading to the formation of example acyl RO₂ radicals. The detailed formation mechanisms
314 of acyl RO₂ measured in this study are shown in Figure S10. The formation of acyl RO₂, especially
315 those having the small molecular size (C₇-C₉), requires the production and subsequent
316 decomposition (or ring-opening process) of RO radicals. Take C₈H₁₃O₆-RO₂ as an example (Figure
317 4), two steps of RO formation and decomposition following the primary C₁₀H₁₅O₄-RO₂ lead to the
318 ring-opened C₈H₁₃O₄-RO₂ that can undergo rapid aldehydic H-shift to form the acyl RO₂. While for
319 C₈H₁₃O₉-RO₂, it directly comes from the aldehydic H-shift of C₈H₁₃O₇-RO followed by the O₂
320 addition (Figure S10).



324

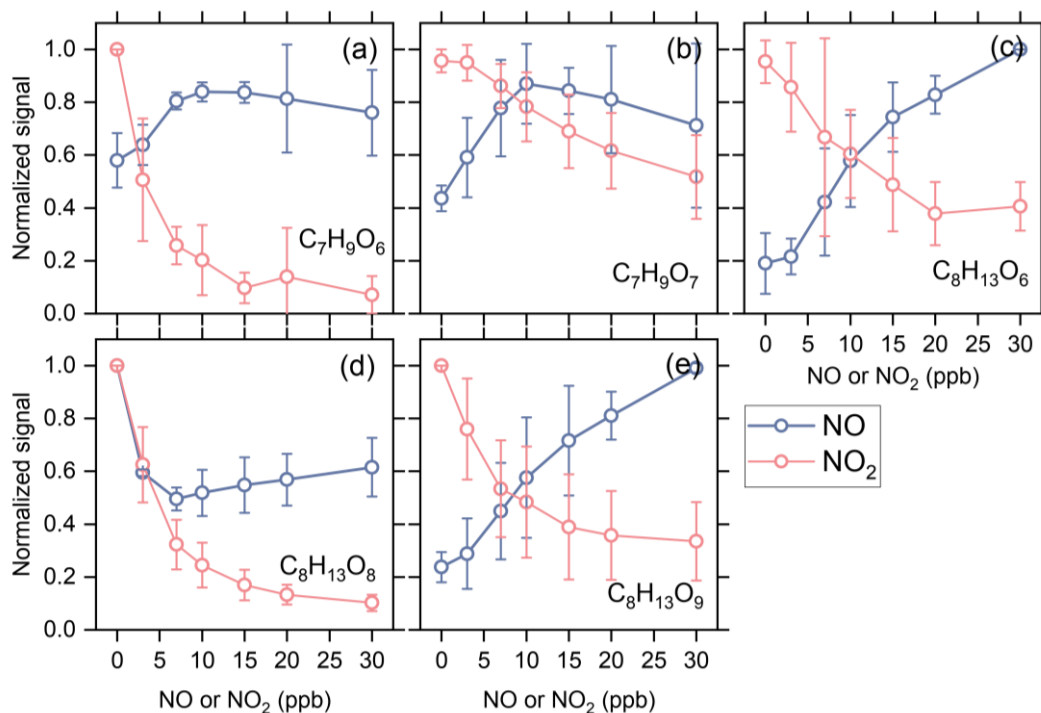


325

326 Figure 4 Three different formation pathways of acyl RO_2 during ozonolysis of α -pinene. The acyl
 327 RO_2 , $C_9H_{13}O_4$ and $C_{10}H_{15}O_5$, formed via pathways 2 and 3, respectively, were not detected by
 328 nitrate-CIMS in this study due to their relatively low oxygenation level.

329 To verify the formation mechanisms of acyl RO_2 , we added NO in some experiments (Exps 33-56)
 330 to see how acyl RO_2 respond to the increasing NO concentration. As shown in Figure 5, the changes
 331 of C_7 and C_8 acyl RO_2 show opposite trend with the increasing NO and NO_2 concentration, except
 332 for $C_8H_{13}O_8-RO_2$. NO can react with RO_2 to form RO radicals and promote the formation of RO_2
 333 that requires the involvement of RO radicals in their formation. In addition to $C_8H_{13}O_6-RO_2$
 334 discussed above, the formation of $C_7H_9O_7-RO_2$ and $C_8H_{13}O_9-RO_2$ needs 2 and 4 steps of the RO
 335 formation following $C_{10}H_{15}O_4-RO_2$ (Figure S10), respectively. Therefore, the increase of RO
 336 concentration due to the addition of NO would promote the production of these acyl RO_2 . These
 337 results prove that the RO radicals indeed play an important role in the acyl RO_2 formation. While
 338 for $C_8H_{13}O_8-RO_2$, its signal decreases substantially with the addition of NO up to 3 ppb, similar to
 339 the trend observed with the addition of NO_2 . After reaching the minimum at 7 ppb NO, the signal
 340 of $C_8H_{13}O_8-RO_2$ tends to increase with the further increase of NO concentration. Given that
 341 $C_8H_{13}O_8-RO_2$ is likely to directly come from the autoxidation of $C_8H_{13}O_6$ acyl RO_2 (see Figure S10),
 342 the rapid consumption of $C_8H_{13}O_6-RO_2$ by NO and NO_2 (formed by O_3 oxidation of NO) may
 343 outcompete its autoxidation process, thus leading to a decrease in $C_8H_{13}O_8-RO_2$ signal. Besides, it
 344 can be seen that the increasing extent in $C_8H_{13}O_6-RO_2$ is also relatively small before the NO
 345 concentration reaches 3 ppb (Figure 5c), indicating that the promotion effect of NO on $C_8H_{13}O_6-$

346 RO₂ formation is not that strong at this concentration.



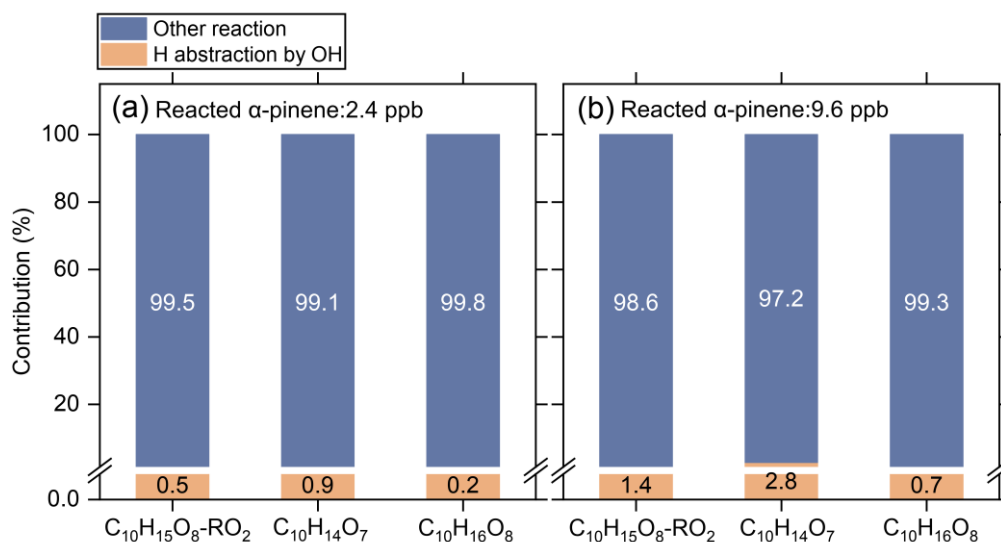
347

348 Figure 5 Averaged normalized signal of typical acyl RO₂ as a function of initial NO or NO₂ addition
349 (Exps 1-28 and 33-56).

350 It is interesting to note that most of the measured highly oxygenated acyl RO₂ are formed by the
351 autoxidation of aldehydic RO₂, and only the C₈H₁₃O₉-RO₂ is formed by the H-shift of the RO radical
352 (Figure S10). The measured signal of acyl RO₂ from the autoxidation pathway accounts for 96% of
353 all highly oxygenated acyl RO₂ signals. Considering that the acyl RO₂ with small molecular size are
354 generally the ring-opened RO₂, the autoxidation rate constant of their precursor RO₂ is expected to
355 be relatively high (e.g., 1 s⁻¹) (Iyer et al., 2021). Taking a RO₂ cross-reaction rate constant of 1 × 10⁻¹²
356 cm³ molecule⁻¹ s⁻¹ (Zhao et al., 2018) and a model-predicted total RO₂ concentration of 1.7 ppb
357 (Exp 8), the simulated contributions of autoxidation and cross-reactions to the total RO₂ reaction
358 are 96.0% and 4.0%, respectively. Considering a 10 times larger RO₂ cross-reaction rate constant
359 (i.e., 1 × 10⁻¹¹ cm³ molecule⁻¹ s⁻¹), the simulated contributions of RO₂ autoxidation and cross-
360 reactions would be 70.4% and 29.6%, respectively. These simulations suggest that the autoxidation
361 of aldehydic RO₂ plays a dominant role in the formation of the highly oxygenated acyl RO₂.
362 Although the acyl RO₂ with low oxygen content were not measured in this study, all acyl RO₂
363 containing oxygen atoms less than 6 seem to be derived from the cleavage of C-C bond or H-shift
364 of RO containing an α-ketone or aldehyde in the currently known reaction mechanisms (Figures 4
365 and S11).

366 Recently, Shen et al. (2022) found that the hydrogen abstraction by OH radicals during α-pinene

367 oxidation plays an important role in HOM formation. In such mechanisms, the primary RO₂ reacts
 368 with NO and forms RO radicals, which could undergo rapid ring-breaking reactions to form a series
 369 of ring-opened C₁₀H₁₅O_x-RO₂, which contains aldehyde functionality and can easily autoxidize to
 370 C₁₀ acyl RO₂. In the absence of NO, the cross-reactions of RO₂ can also produce RO radicals.
 371 However, only a few C₁₀ acyl RO₂ were detected in this study and they contribute less than 1% of
 372 the total C₁₀ RO₂ signal. This phenomenon could be due to the fact that the primary RO₂ (C₁₀H₁₅O₂)
 373 formed by the hydrogen abstraction by OH radical are least-oxidized with only 2 oxygen atoms,
 374 which are expected to have a relatively low cross-reaction rate constant (Orlando and Tyndall, 2012;
 375 Berndt et al., 2018). As a result, the formation of ring-opened C₁₀H₁₅O_x-RO₂ via cross-reactions of
 376 the primary C₁₀H₁₅O₂-RO₂ may not be important. As shown in Figure 6, when the cross-reaction
 377 rate constants of C₁₀H₁₅O₂-RO₂ is considered to be 1 × 10⁻¹³ cm³ molecule⁻¹ s⁻¹, the simulated
 378 contribution of the H-abstraction pathway to the HOM formation is less than 3% under both low
 379 (2.4 ppb) and high (9.6 ppb) reacted α-pinene conditions. It should be note that the cross-reaction
 380 rate constants of the less-oxygenated RO₂ could be even lower (Orlando and Tyndall, 2012),
 381 therefore the contribution of this pathway to HOM formation could be ignored when NO is absent.

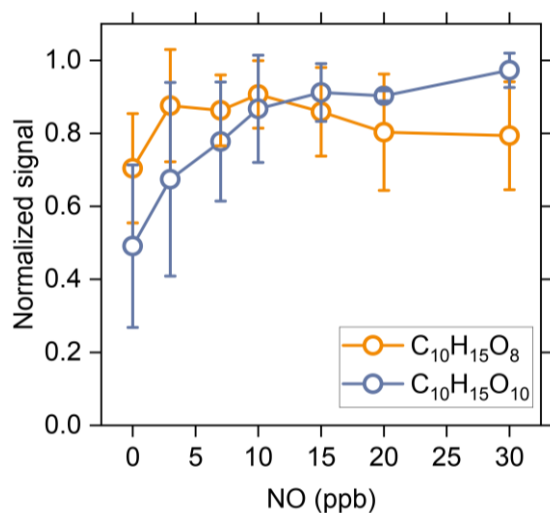


382

383 Figure 6 Contributions of the H-abstraction pathways by OH radicals (yellow) and OH addition and
 384 ozonolysis pathways (blue) to the formation of typical HOMs under low (a) and high (b) reacted α-
 385 pinene conditions simulated by the kinetic model. The cross-reaction rate constant was set to 1 ×
 386 10⁻¹³ cm³ molecule⁻¹ s⁻¹ for the primary C₁₀H₁₅O₂-RO₂ and 1 × 10⁻¹² cm³ molecule⁻¹ s⁻¹ for the more
 387 oxygenated RO₂.

388 In the presence of cyclohexane as an OH scavenger (Figure S12, Exp 32), the measured signals of
 389 C₁₀H₁₇O_x-RO₂ formed via OH addition channel and the corresponding C₁₀H₁₈O_x-HOMs decrease
 390 by more than 70%, while the C₁₀H₁₅O_x-RO₂ and its related closed-shell products decrease by less

391 than 15%, in good agreement with the measurements in previous studies (Zhao et al., 2018). As the
392 $C_{10}H_{16}O_8$ -HOM could come from both $C_{10}H_{15}O_x$ -RO₂ and $C_{10}H_{17}O_x$ -RO₂, its reduction is at a
393 medium level. The significantly smaller decrease in the signals of $C_{10}H_{15}O_x$ -RO₂ and its
394 corresponding closed-shell products as compared to those of $C_{10}H_{17}O_x$ -RO₂ and the related closed-
395 shell products further illustrates that the H-abstraction by OH has a minor contribution to HOM
396 formation in the absence of NO.



397

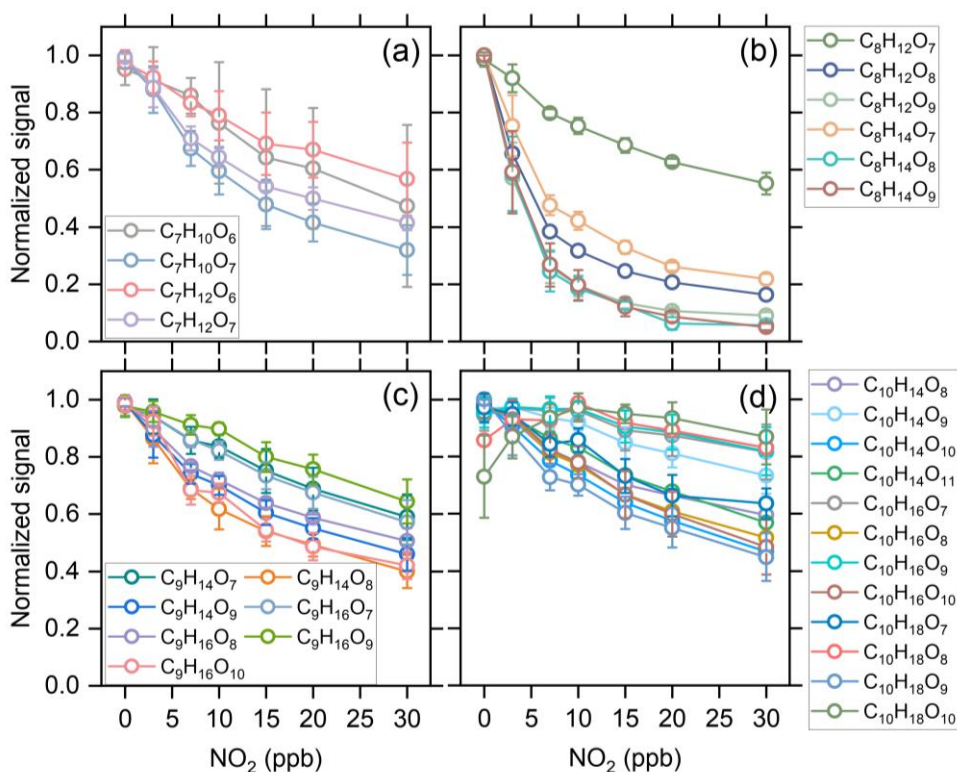
398 Figure 7 Averaged normalized signal of the measured $C_{10}H_{15}O_8$ - and $C_{10}H_{15}O_{10}$ -RO₂ as a function
399 of the added NO concentration (Exps 33-56).

400 Figure 7 shows the changes in measured signal of $C_{10}H_{15}O_8$ -RO₂ and $C_{10}H_{15}O_{10}$ -RO₂ as a function
401 of initial NO concentration (Exps 33-56). It should be noted that due to the existence of O₃ in our
402 experiments, these two RO₂ could come from both O₃ and OH reactions with α -pinene and NO
403 could be rapidly oxidized to NO₂ by O₃. The normalized signals of $C_{10}H_{15}O_8$ -RO₂ and $C_{10}H_{15}O_{10}$ -
404 RO₂ increase firstly under low NO conditions, which is similar to the change of acyl RO₂ as shown
405 in Figure 5. This increase could be due to two reasons: (1) the promoted formation of $C_{10}H_{15}O_8$ and
406 $C_{10}H_{15}O_{10}$ acyl RO₂ from the H-abstraction channel by NO addition and (2) the equilibrium
407 decomposition of ROONO₂ formed by the two alkyl RO₂ from ozonolysis of α -pinene in the
408 chemical ionization inlet (see Section 3.1). As mentioned above, the ring-opened $C_{10}H_{15}O_x$ -RO₂
409 formed from the H-abstraction channel contain aldehyde functionality and can autoxidize rapidly.
410 The F0AM model simulations show that the $C_{10}H_{15}O_8$ and $C_{10}H_{15}O_{10}$ acyl RO₂ formed from the H-
411 abstraction channel contribute to 68% and 56% of the total $C_{10}H_{15}O_8$ -RO₂ and $C_{10}H_{15}O_{10}$ -RO₂ with
412 the addition of 10 ppb NO, respectively. Therefore, the initial increases of these two RO₂ with
413 increasing NO concentration are likely mainly due to the enhanced formation of $C_{10}H_{15}O_8$ and
414 $C_{10}H_{15}O_{10}$ acyl RO₂. When the NO concentration increases to a high level, there are more NO and
415 NO₂ in the system, which promotes the consumption of acyl RO₂. As a result, $C_{10}H_{15}O_8$ -RO₂

416 exhibits a decreasing trend and the increasing extend of $C_{10}H_{15}O_{10}$ -RO₂ becomes much smaller.

417 3.3 Contributions of acyl RO₂ to the formation of gas-phase HOMs

418 With the addition of NO₂, the distribution of gas-phase products in the α -pinene ozonolysis changes
419 significantly (see Figure 1), and the consumption of acyl RO₂ by NO₂ plays an important role. NO₂
420 influences the formation of HOM monomers mainly in three ways. Firstly, NO₂ could react rapidly
421 with acyl RO₂ and form RC(O)OONO₂, thus inhibiting the formation of HOMs with the
422 involvement of acyl RO₂. Secondly, as mentioned above, although ROONO₂ is thermally unstable,
423 their formation/decomposition equilibrium still consumes a small amount of alkyl RO₂, resulting in
424 a decrease in HOM formation. Thirdly, NO₂ can consume a part of HO₂ radicals (Figure S13), thus
425 inhibiting the RO₂ + HO₂ reaction pathway.



426

427 Figure 8 Averaged normalized signal of the measured C₇-C₁₀ HOMs as a function of the added NO₂
428 concentration (Exps 1-28).

429 Figure 8 shows the normalized signal of C₇-C₁₀ HOM monomers as a function of initial NO₂
430 concentration. The signals of C₇, C₈, and some of C₉ HOMs decrease significantly with increasing
431 NO₂ concentration due to the relatively large contribution of acyl RO₂ to the total C₇-C₉ RO₂. The
432 C₇ HOMs decrease by more than 50% when the NO₂ concentration reaches 30 ppb, while C₈ HOMs
433 decrease by more than 70% and some of them even decrease by 90%. The C₉ HOMs decrease by
434 30%-60% and the species with relatively large decrease are mostly acyl RO₂-related HOMs. For

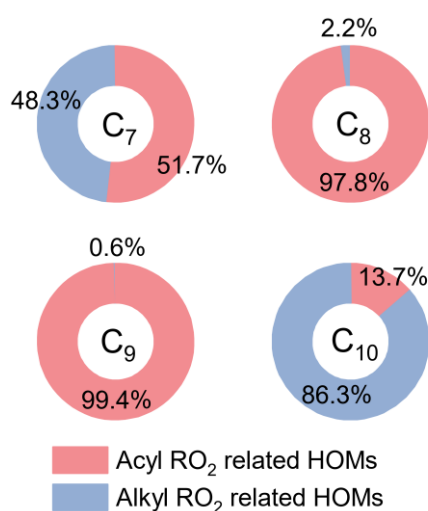
435 C₁₀ HOMs, although there is also an obvious decrease in their formation with the addition of NO₂,
436 most of them have a smaller decreasing extent compared to the C₇-C₉ HOMs due to the low
437 contribution of acyl RO₂ to the C₁₀ RO₂. It is worth noting that a few C₁₀ HOMs increase initially
438 with the addition of NO₂ up to 10 ppb, suggesting that there might be some processes that promote
439 the formation of their precursor RO₂ radicals and thus offset the inhibiting effect of NO₂.

440 As mentioned above, the addition of NO₂ has the most significant influence on the formation of
441 small HOM monomers. Combined with the large contribution (67-94%) of acyl RO₂ to the total C₇
442 and C₈ RO₂ (Figure 3), it can be considered that the reduction in the formation of C₇ and C₈ HOM
443 monomers with NO₂ addition is overwhelmingly due to the consumption of acyl RO₂ by NO₂. As a
444 result, acyl RO₂ was found to have a contribution of 50-90% to C₇ and C₈ HOM monomer formation
445 during α -pinene ozonolysis. Since acyl RO₂ also have a considerable contribution (32%) to the total
446 C₉ RO₂, an upper limit (30%-60%) of its contribution to C₉ HOMs could be derived with the
447 assumption that the decrease of C₉ HOMs with the addition of NO₂ is also mainly due to the
448 consumption of C₉-acyl RO₂ by NO₂. By contrast, acyl RO₂ account for a very small fraction (0.4%)
449 of the total C₁₀ RO₂, and their contribution to C₁₀ HOMs cannot be quantified based solely on the
450 experimental measurements given that the equilibrium reaction between alkyl RO₂ and NO₂ can
451 also affect the formation of HOMs. Therefore, we used the FOAM model to simulate the contribution
452 of acyl RO₂ to C₁₀ HOM formation according to the acyl RO₂ measured in this study and displayed
453 the results in Figure 9. It should be noted that the HOMs from the acyl RO₂ and its subsequent RO₂
454 (formed from acyl RO₂ reactions) are all considered as acyl RO₂-related HOMs in the model.

455 As mentioned above, the formation of ring-opened C₁₀H₁₅O₄-RO₂ reported by Iyer et al. (2021) is
456 included in the model, and its autoxidation produces a ring-opened acyl C₁₀H₁₅O₈-RO₂. When we
457 consider the upper limit of the yield of ring-opened C₁₀H₁₅O₄-RO₂ (89%) in the model and assume
458 that the other primary RO₂ with the cyclobutyl ring autoxidize at a very slow rate (0.01 s⁻¹), the
459 simulated acyl C₁₀H₁₅O₈-RO₂ would contribute to ~80% of the total C₁₀ RO₂. However, we could
460 not see a large decrease in the measured signal of C₁₀H₁₅O₈-RO₂ and its related HOM monomers
461 with the addition of NO₂. Similarly, a recent study by Zhao et al. (2022) found that the C₁₀H₁₅O₈-
462 related monomers and dimers in α -pinene SOA did not significantly decrease with NO₂ addition.
463 There might be three reasons for the discrepancy between the simulations and measurements. Firstly,
464 the yield of the ring-opened C₁₀H₁₅O₄-RO₂ might be significantly smaller than 89% (Zhao et al.,
465 2021; Meder et al., 2023). Secondly, the autoxidation rate of other primary C₁₀H₁₅O₄-RO₂ with the
466 cyclobutyl ring could be significantly larger than 0.01 s⁻¹. Thirdly, the ring-opened C₁₀H₁₅O₈-RO₂,
467 a highly functionalized acyl RO₂ radical with an -OOH group, may be able to undergo very fast

468 intramolecular H-scrambling reactions to form a peroxy acid as suggested by Knap and Jørgensen,
469 (2017), which would compete with the NO₂ reaction and result in a lower reduction in its signal
470 upon NO₂ addition (see details in Section S3).

471 To examine the contributions of acyl RO₂ to C₁₀ HOM production, we updated the branching ratios
472 and autoxidation rates of the primary RO₂ during α -pinene ozonolysis in the model according to the
473 recent studies (Kurten et al., 2015; Clafin et al., 2018; Zhao et al., 2021; Berndt, 2022) (Table S3),
474 and used a lower limit (30%) of the ring-opened C₁₀H₁₅O₄-RO₂ yield reported by Iyer et al. (2021).
475 The simulated acyl RO₂-related HOMs contribute to 14% of the total C₁₀ HOMs, which is slightly
476 smaller than the measured decrease in C₁₀ HOMs with the addition of NO₂. This discrepancy could
477 be due to two reasons. Firstly, the decrease in HOMs can partly result from the consumption of alkyl
478 RO₂ and HO₂ radicals by the addition of NO₂. Secondly, as mentioned above, there might be other
479 C₁₀ acyl RO₂ that were not observed in this study due to the decomposition of the ROONO₂ from
480 the alkyl RO₂ with the same formulas. The contributions of acyl RO₂ to the formation of C₇-C₉
481 HOMs were also simulated (Figure 9). For C₇ and C₈ HOMs, the model predicts a contribution of
482 52%-98% from acyl RO₂, which is consistent with the measurements (50%-90%). However, the
483 simulated contribution of acyl RO₂ to C₉ HOMs is over 99%, which is not consistent with the
484 measurements (Figure 8c). Recent studies indicated that the CI radicals from α -pinene ozonolysis
485 could not form the alkyl C₉H₁₅O₃-RO₂ (C96O2 in default MCM v3.3.1) (Kurten et al., 2015; Zhao
486 et al., 2021; Berndt, 2022). As a result, this primary C₉ alkyl RO₂ was not considered in the model,
487 and most of C₉ RO₂ considered are acyl RO₂ or from acyl RO₂ reactions. In view of the significantly
488 lower measured (less than 30-60%) than simulated (over 99%) contribution of acyl RO₂ to C₉ HOMs,
489 we speculate that a small part of CI radicals might be able to form the C₉H₁₅O₃-RO₂, which could
490 further react to form highly oxygenated alkyl C₉ RO₂.



491

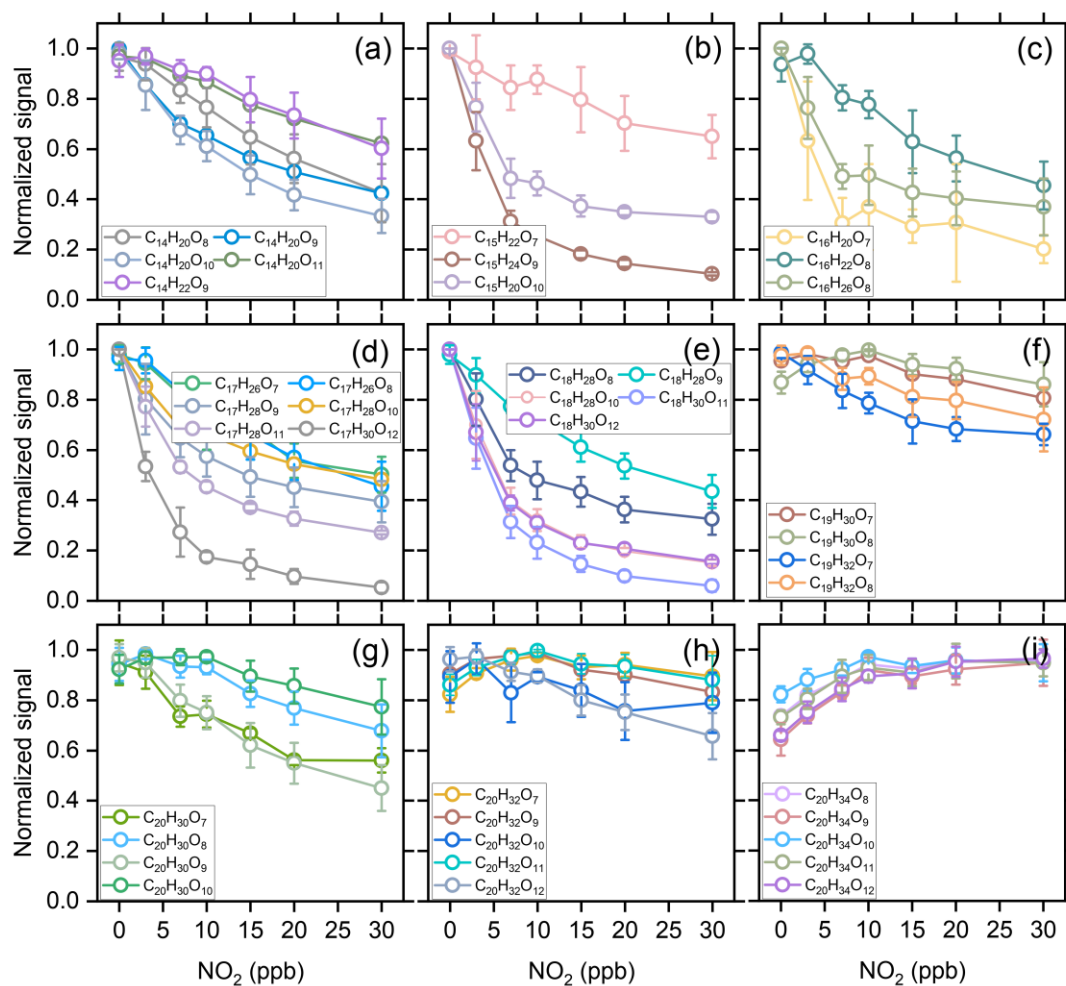
492 Figure 9 Simulated average contribution of acyl and alkyl RO₂ to C₇-C₁₀ HOM formation from
493 ozonolysis of α-pinene under typical experimental conditions (Exps 1, 8, 15, and 22).

494 A sensitivity analysis of the alkyl C₉H₁₅O₃-RO₂ yield was conducted to see its influence on the
495 contribution of acyl RO₂ to the total C₉ HOMs. The model simulations show that when the yield of
496 this C₉ RO₂ from one of the CIs ranges between 0.5% to 2%, the contribution of acyl RO₂ to the
497 total C₉ HOMs ranges from 27.5% to 59.8% (Figure S15), which is almost consistent with the
498 measurements. This result indicates that a small part of CIs could generate the C₉ alkyl RO₂. We
499 note that the small production of C₉H₁₅O₃-RO₂ from CIs has no significant influence on the yield
500 of C₁₀H₁₅O₄-RO₂ and the subsequent acyl RO₂. As shown in Figure S16, as the C₉H₁₅O₃-RO₂ yield
501 increases from 0% to 3%, the simulated concentrations of C₁₀H₁₅O₄-RO₂ exhibit negligible to small
502 (5%) changes. As the C₉H₁₅O₃-RO₂ is considered to only produce highly oxygenated alkyl RO₂ in
503 the model, it results in a decrease in the contribution of acyl RO₂ to the total C₉ HOMs. However,
504 the contributions of acyl RO₂ to total C₇, C₈, and C₁₀ HOMs are almost unchanged.

505 The cross-reaction rate constant of acyl RO₂ is generally larger than that of alkyl RO₂ (Atkinson et
506 al., 2007; Orlando and Tyndall, 2012), and the fast cross-reaction may lead to an important
507 contribution to the HOM dimer production. The responses of dimer formation to increasing
508 concentration of initial NO₂ during α-pinene ozonolysis are given in Figure 10. The C₁₄-C₁₈ dimers
509 decrease by up to 50%-95% with the increase of NO₂ concentration up to 30 ppb (Figures 10a-e).
510 The rapid cross-reaction rate of acyl RO₂, as well as their dominant contribution to the small RO₂
511 species makes acyl RO₂ an important contributor to the formation of these dimers. The consumption
512 of acyl RO₂ by NO₂ greatly inhibits the bimolecular reactions involving acyl RO₂, resulting in a
513 rapid decrease in the signal of the corresponding dimers. Considering the predominance of acyl RO₂
514 in small RO₂ and their high reaction rate with NO₂ compared to the alkyl RO₂, it can be concluded
515 that the cross-reactions involving acyl RO₂ contribute to roughly 50%-95% of the C₁₄-C₁₈ dimer
516 formation.

517 For C₁₉ dimers, due to the relatively smaller contribution of acyl RO₂ to C₉ and C₁₀ RO₂, their signal
518 decreases only by 10%-40%, and this reduction have contributions from both acyl and alkyl RO₂.
519 For C₂₀ dimers, their signal changes with the addition of NO₂ can be discussed according to the
520 number of hydrogen atoms in the molecules. Firstly, the signals of C₂₀H₃₀O₇ and C₂₀H₃₀O₉ decrease
521 by 40-60% with the addition of 30 ppb NO₂, indicating a significant contribution of acyl RO₂ such
522 as C₁₀H₁₅O₅-RO₂ (acyl RO₂ in default MCM v3.3.1) and C₁₀H₁₅O₇-RO₂ in their formation, while
523 other C₂₀H₃₀O_x dimers decrease by ~30%. The C₂₀H₃₂O_x dimer series also exhibits a small reduction
524 (less than 20%) with the addition of NO₂. However, the C₂₀H₃₄O_x series shows an unexpected

525 increase with the addition of NO₂ up to 10 ppb and almost remains unchanged with the further
 526 increase of NO₂ concentration. Given that the cross-reaction rate constant of acyl RO₂ can be orders
 527 of magnitude higher than that of counterpart alkyl RO₂ (Atkinson et al., 2007; Orlando and Tyndall,
 528 2012), the rapid consumption of acyl RO₂ by NO₂ would preserve the alkyl RO₂ that tend to react
 529 with acyl RO₂ at a fast rate in the absence of NO₂, which to some extent would elevate the
 530 concentration of alkyl RO₂ in the system and thus promote the less competitive alkyl RO₂ + alkyl
 531 RO₂ reactions to form C₂₀H₃₄O_x dimers. The slight increase of some C₁₀H₁₈O_x-HOMs with the
 532 addition of NO₂ up to 10 ppb could also be due to this reason.

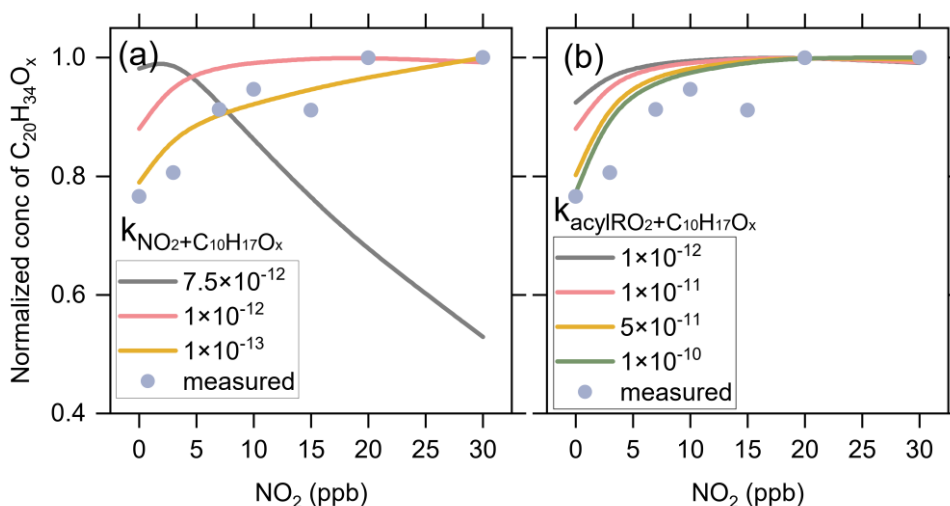


533
 534 Figure 10 Averaged normalized signal of the measured C₁₄-C₂₀ dimers as a function of the added
 535 NO₂ concentration (Exps 1-28).

536 According to the noticeable increasing trend in C₂₀H₃₄O_x as compared to other C₂₀ dimers, we
 537 speculate that acyl RO₂ react faster with C₁₀H₁₇O_x alkyl RO₂ than with C₁₀H₁₅O_x alkyl RO₂.
 538 Therefore, when the acyl RO₂ is depleted, the preservation of C₁₀H₁₇O_x-RO₂ is more significant and
 539 the promotion of their cross-reactions to form C₂₀H₃₄O_x is more evident. It is also possible that the

540 reaction of NO_2 with $\text{C}_{10}\text{H}_{17}\text{O}_x$ alkyl RO_2 is less efficient compared to the reaction with $\text{C}_{10}\text{H}_{15}\text{O}_x$
 541 alkyl RO_2 , so more $\text{C}_{10}\text{H}_{17}\text{O}_x$ than $\text{C}_{10}\text{H}_{15}\text{O}_x$ are available for dimer formation in the presence of
 542 NO_2 .

543 To further prove the above two speculations, we performed sensitivity analyses for the reaction rates
 544 of $\text{C}_{10}\text{H}_{17}\text{O}_x\text{-RO}_2$ using the F0AM model. Figures 11a show the changes in $\text{C}_{20}\text{H}_{34}\text{O}_x$ dimers with
 545 NO_2 addition at different $\text{C}_{10}\text{H}_{17}\text{O}_x\text{-RO}_2 + \text{NO}_2$ reaction rates under the conditions of Exps 8-14. As
 546 the reaction rate varies from 1×10^{-13} to 1×10^{-12} $\text{cm}^3 \text{ molecule}^{-1} \text{ s}^{-1}$, the increasing trend of $\text{C}_{20}\text{H}_{34}\text{O}_x$
 547 dimers versus the added NO_2 concentration is weakened and the simulation is more deviated from
 548 the measurements. When the reaction rate increases to 7.5×10^{-12} $\text{cm}^3 \text{ molecule}^{-1} \text{ s}^{-1}$, the $\text{C}_{20}\text{H}_{34}\text{O}_x$
 549 dimers decrease significantly with increasing NO_2 , which is in striking contrast to the measurements.
 550 Figure 11b presents the sensitivity analysis results for the cross-reaction rate constants of acyl RO_2
 551 + $\text{C}_{10}\text{H}_{17}\text{O}_x\text{-RO}_2$. As this rate constant varies from 1×10^{-12} to 1×10^{-10} $\text{cm}^3 \text{ molecule}^{-1} \text{ s}^{-1}$, the
 552 increasing trend of $\text{C}_{20}\text{H}_{34}\text{O}_x$ versus the NO_2 concentration is more pronounced and more consistent
 553 with the measurements. These sensitivity analyses support our speculation that the $\text{C}_{10}\text{H}_{17}\text{O}_x$ alkyl
 554 RO_2 may be different from other alkyl RO_2 radicals in terms of the reaction efficiency with NO_2 and
 555 acyl RO_2 species, which leads to different responses of $\text{C}_{20}\text{H}_{34}\text{O}_x$ dimers to NO_2 addition compared
 556 to other C_{20} dimers. These results also suggest that the presence of acyl RO_2 could affect the fate
 557 and contribution of alkyl RO_2 to HOM formation in atmospheric oxidation systems given the
 558 different reactivity of acyl RO_2 from alkyl RO_2 .



559
 560 Figure 11 Sensitivity of $\text{C}_{20}\text{H}_{34}\text{O}_x$ dimer production to (a) the reaction rates of NO_2 with $\text{C}_{10}\text{H}_{17}\text{O}_x\text{-}$
 561 RO_2 and (b) the cross-reaction rate of acyl RO_2 with $\text{C}_{10}\text{H}_{17}\text{O}_x\text{-RO}_2$ considering a $\text{C}_{10}\text{H}_{17}\text{O}_x\text{-RO}_2 +$
 562 NO_2 reaction rate of 1×10^{-12} $\text{cm}^3 \text{ molecule}^{-1} \text{ s}^{-1}$.

563 4. Conclusions

564 In this study, the molecular identities, formation mechanisms, and contributions of acyl RO₂ to the
565 formation of HOMs during ozonolysis of α -pinene are investigated using a combination of flow
566 reactor experiments and detailed kinetic model simulations. Based on the marked decrease in RO₂
567 signal as a function of initial NO₂ concentration, a total of 10 acyl RO₂ are identified during α -
568 pinene ozonolysis. The acyl RO₂ contributes to 67%, 94% and 32% of C₇, C₈ and C₉ highly
569 oxygenated RO₂ but only 0.4% of C₁₀ highly oxygenated RO₂, respectively. Three main pathways
570 are identified for the formation of monoterpene-derived acyl RO₂: (i) the autoxidation of RO₂
571 containing aldehyde groups, (ii) the cleavage of C-C bond of RO containing an α -ketone group, and
572 (iii) the intramolecular H-shift of RO containing an aldehyde group. The autoxidation of aldehydic
573 RO₂ formed involving multiple RO decomposition or ring-opening steps plays a dominant role in
574 the formation of the highly oxygenated acyl RO₂ radicals (oxygen atom number ≥ 6), while the less-
575 oxygenated acyl RO₂ (oxygen atom number < 6) are mainly derived from the other two pathways.

576 The acyl RO₂-involved reactions explain 50-90% of C₇ and C₈ HOM monomers and 14% of C₁₀
577 HOMs, respectively. For C₉ HOMs, this contribution can be up to 30%-60%. For the HOM dimers,
578 acyl RO₂-involved reactions contribute 50%-95% to the formation of C₁₄-C₁₈ dimers. Owing to the
579 higher cross-reaction rate constant of acyl RO₂ compared to alkyl RO₂, the acyl RO₂ + alkyl RO₂
580 reaction would outcompete the alkyl RO₂ + alkyl RO₂ reaction. Therefore, the rapid consumption
581 of acyl RO₂ by NO₂ in the experiments (as well as in polluted atmospheres) would make the alkyl
582 RO₂ that are supposed to react with acyl RO₂ retained, which to some extent elevates the
583 concentration of alkyl RO₂ in the system and thus promotes the reaction of alkyl RO₂ + alkyl RO₂
584 to form dimers such as C₂₀H₃₄O_x. The contribution of H-abstraction of α -pinene by OH radical to
585 the formation of acyl RO₂ and HOMs is found to be negligible in the absence of NO. This is because
586 the primary C₁₀H₁₅O₂-RO₂ radicals formed in such pathways are least-oxidized and thus have
587 relatively low cross-reaction efficiency to produce RO radicals, which are the key intermediates for
588 the formation of acyl RO₂ and HOMs in that channel. However, in the presence of NO, the formation
589 of highly oxygenated acyl RO₂ via the H-abstraction pathway is demonstrated, consistent with
590 previous studies (Shen et al., 2022).

591 In this study, acyl RO₂ species are identified according to a dramatic decrease in their signal with
592 the addition of NO₂. It should be noted that the presence of NO₂ could also inhibit the formation of
593 alkyl RO₂ species involving acyl RO₂ reactions. If there are any contributions of alkyl RO₂ to acyl
594 RO₂ identified in this study, the influence of such alkyl RO₂ species on HOM formation would
595 reflect an indirect effect of acyl RO₂. However, given that the formation of most of the acyl RO₂

596 identified in this study can be reasonably explained by the proposed mechanisms and verified by
597 their responses to the addition of NO, the acyl RO₂ identified here are expected to have no significant
598 contributions from alkyl RO₂. Currently, the reaction kinetics of monoterpene-derived acyl RO₂ are
599 still poorly understood. Considering the important contribution of acyl RO₂ to HOM formation,
600 further kinetic studies are needed to get more specific rate constants for their autoxidation and cross-
601 reactions, thereby deepening our understanding of the role of acyl RO₂ in HOM and SOA formation
602 under atmospheric conditions.

603

604 *Data availability.* The data presented in this work are available upon request from the corresponding
605 author.

606

607 *Author contributions.* YZ and HZ designed the study, HZ, DH and JZ performed the experiments.
608 YZ and HZ analyzed the data, conducted model simulations, and wrote the paper. All other authors
609 contributed to discussion and writing.

610

611 *Competing interests.* The authors declare no conflict of interest.

612

613 *Acknowledgments.* Yue Zhao acknowledges the Program for Professor of Special
614 Appointment (Eastern Scholar) at Shanghai Institutions of Higher Learning.

615

616 *Financial support.* This work was supported by the National Natural Science Foundation
617 of China (grants 22022607, 21806104, and 42005090) and the Program for Professor of
618 Special Appointment (Eastern Scholar) at Shanghai Institutions of Higher Learning.

619

620 **References**

621 Atkinson, R., Hasegawa, D., and Aschmann, S. M.: Rate constants for the gas-phase reactions of O₃ with
622 a series of monoterpenes and related compounds at 296 ± 2 K, *Int. J. Chem. Kinet.*, 1221,
623 <https://doi.org/10.1002/kin.550220807>, 1990.

624 Atkinson, R., Baulch, D., Cox, R., Crowley, J., Hampson, R., Hynes, R., Jenkin, M., Rossi, M., and Troe,
625 J.: Evaluated kinetic and photochemical data for atmospheric chemistry: Volume III—gas phase
626 reactions of inorganic halogens, *Atmos. Chem. Phys.*, 7, 981-1191, [https://doi.org/10.5194/acp-7-](https://doi.org/10.5194/acp-7-981-2007)
627 981-2007, 2007.

628 Bell, D. M., Wu, C., Bertrand, A., Graham, E., Schoonbaert, J., Giannoukos, S., Baltensperger, U., Prevot,
629 A., Riipinen, I., and Haddad, I. E.: Particle-phase processing of α-pinene NO₃ secondary organic
630 aerosol in the dark, *Atmos. Chem. Phys.*, 13167–13182, [https://doi.org/10.5194/acp-22-13167-](https://doi.org/10.5194/acp-22-13167-2022)
631 2022, 2021.

632 Berndt, T.: Peroxy radical processes and product formation in the OH radical-initiated oxidation of alpha-
633 pinene for near-atmospheric conditions, *J. Phys. Chem. A*, 125, 9151-9160,
634 <https://doi.org/10.1021/acs.jpca.1c05576>, 2021.

635 Berndt, T.: Peroxy radical and product formation in the gas-phase ozonolysis of alpha-pinene under near-

636 atmospheric conditions: occurrence of an additional series of peroxy radicals O₂O-
637 C₁₀H₁₅O(O₂)_yO₂ with y = 1-3, *J. Phys. Chem. A*, 126, 6526-6537,
638 <https://doi.org/10.1021/acs.jpca.2c05094>, 2022.

639 Berndt, T., Mentler, B., Scholz, W., Fischer, L., Herrmann, H., Kulmala, M., and Hansel, A.: Accretion
640 product formation from ozonolysis and OH radical reaction of alpha-pinene: mechanistic insight
641 and the influence of isoprene and ethylene, *Environ. Sci. Technol.*, 52, 11069-11077,
642 <https://doi.org/10.1021/acs.est.8b02210>, 2018.

643 Berndt, T., Richters, S., Jokinen, T., Hyttinen, N., Kurtén, T., Otkjær, R. V., Kjaergaard, H. G., Stratmann,
644 F., Herrmann, H., and Sipilä, M.: Hydroxyl radical-induced formation of highly oxidized organic
645 compounds, *Nat. Commun.*, 7, 1-8, <https://doi.org/10.1038/ncomms13677>, 2016.

646 Bianchi, F., Kurtén, T., Riva, M., Mohr, C., Rissanen, M. P., Roldin, P., Berndt, T., Crouse, J. D.,
647 Wennberg, P. O., and Mentel, T. F.: Highly oxygenated organic molecules (HOM) from gas-phase
648 autoxidation involving peroxy radicals: A key contributor to atmospheric aerosol, *Chem. Rev.*, 119,
649 3472-3509, 2019.

650 Calvert, J. G., Derwent, R. G., Orlando, J. J., Wallington, T. J., and Tyndall, G. S.: Mechanisms of
651 atmospheric oxidation of the alkanes, 2008.

652 Clafflin, M. S., Krechmer, J. E., Hu, W., Jimenez, J. L., and Ziemann, P. J.: Functional group composition
653 of secondary organic aerosol formed from ozonolysis of α -pinene under high VOC and autoxidation
654 conditions, *ACS Earth Space Chem.*, 2, 1196-1210,
655 <https://doi.org/10.1021/acsearthspacechem.8b00117>, 2018.

656 Ehn, M., Thornton, J. A., Kleist, E., Sipilä, M., Junninen, H., Pullinen, I., Springer, M., Rubach, F.,
657 Tillmann, R., and Lee, B.: A large source of low-volatility secondary organic aerosol, *Nature*, 506,
658 476-479, <https://doi.org/10.1038/nature13032>, 2014.

659 Fry, J., Kiendler-Scharr, A., Rollins, A., Wooldridge, P., Brown, S., Fuchs, H., Dubé, W., Mensah, A., Dal
660 Maso, M., and Tillmann, R.: Organic nitrate and secondary organic aerosol yield from NO₃
661 oxidation of β -pinene evaluated using a gas-phase kinetics/aerosol partitioning model, *Atmos.*
662 *Chem. Phys.*, 9, 1431-1449, <https://doi.org/10.5194/acp-9-1431-2009>, 2009.

663 Fry, J. L., Draper, D. C., Barsanti, K. C., Smith, J. N., Ortega, J., Winkler, P. M., Lawler, M. J., Brown,
664 S. S., Edwards, P. M., and Cohen, R. C.: Secondary organic aerosol formation and organic nitrate
665 yield from NO₃ oxidation of biogenic hydrocarbons, *Environ. Sci. Technol.*, 48, 11944-11953,
666 <https://doi.org/10.1021/es502204x>, 2014.

667 Guenther, A., Jiang, X., Heald, C. L., Sakulyanontvittaya, T., Duhl, T. a., Emmons, L., and Wang, X.:
668 The model of emissions of gases and aerosols from nature version 2.1 (MEGAN2. 1): an extended
669 and updated framework for modeling biogenic emissions, *Geosci. Model Dev.*, 5, 1471-1492,
670 <https://doi.org/10.5194/gmd-5-1471-2012>, 2012.

671 Iyer, S., Rissanen, M. P., Valiev, R., Barua, S., Krechmer, J. E., Thornton, J., Ehn, M., and Kurten, T.:
672 Molecular mechanism for rapid autoxidation in alpha-pinene ozonolysis, *Nat. Commun.*, 12, 878,
673 <https://doi.org/10.1038/s41467-021-21172-w>, 2021.

674 Jenkin, M., Young, J., and Rickard, A.: The MCM v3.3.1 degradation scheme for isoprene, *Atmos. Chem.*
675 *Phys.*, 15, 11433-11459, <https://doi.org/10.5194/acp-15-11433-2015>, 2015.

676 Jokinen, T., Sipilä, M., Richters, S., Kerminen, V. M., Paasonen, P., Stratmann, F., Worsnop, D., Kulmala,
677 M., Ehn, M., and Herrmann, H.: Rapid autoxidation forms highly oxidized RO₂ radicals in the
678 atmosphere, *Angew. Chem. Int. Ed.*, 53, 14596-14600, <https://doi.org/10.1002/anie.201408566>,
679 2014.

680 Junninen, H., Ehn, M., Petäjä, T., Luosujärvi, L., Kotiaho, T., Kostianen, R., Rohner, U., Gonin, M.,
681 Fuhrer, K., and Kulmala, M.: A high-resolution mass spectrometer to measure atmospheric ion
682 composition, *Atmos. Meas. Tech.*, 3, 599-636, <https://doi.org/10.5194/amt-3-1039-2010>, 2010.

683 Kirchner, F., Thuener, L., Barnes, I., Becker, K., Donner, B., and Zabel, F.: Thermal lifetimes of
684 peroxy nitrates occurring in the atmospheric degradation of oxygenated fuel additives, *Environ. Sci.*
685 *Technol.*, 31, 1801-1804, <https://doi.org/10.1021/es9609415>, 1997.

686 Knap, H. C. and Jørgensen, S.: Rapid Hydrogen Shift Reactions in Acyl Peroxy Radicals, *J. Phys. Chem.*
687 *A*, 121, 1470-1479, [10.1021/acs.jpca.6b12787](https://doi.org/10.1021/acs.jpca.6b12787), 2017.

688 Knopf, D. A., Pöschl, U., and Shiraiwa, M.: Radial diffusion and penetration of gas molecules and aerosol
689 particles through laminar flow reactors, denuders, and sampling tubes, *Anal. Chem.*, 87, 3746-3754,
690 <https://doi.org/10.1021/ac5042395>, 2015.

691 Kristensen, K., Watne, Å. K., Hammes, J., Lutz, A., Petäjä, T., Hallquist, M., Bilde, M., and Glasius, M.:
692 High-molecular weight dimer esters are major products in aerosols from α -pinene ozonolysis and
693 the boreal forest, *Environ. Sci. Technol. Lett.*, 3, 280-285, 2016.

694 Kurten, T., Rissanen, M. P., Mackeprang, K., Thornton, J. A., Hyttinen, N., Jørgensen, S., Ehn, M., and
695 Kjaergaard, H. G.: Computational study of hydrogen shifts and ring-opening mechanisms in alpha-
696 pinene ozonolysis products, *J. Phys. Chem. A*, 119, 11366-11375,
697 <https://doi.org/10.1021/acs.jpca.5b08948>, 2015.

698 Li, X., Chee, S., Hao, J., Abbatt, J. P. D., Jiang, J., and Smith, J. N.: Relative humidity effect on the
699 formation of highly oxidized molecules and new particles during monoterpene oxidation, *Atmos.*
700 *Chem. Phys.*, 19, 1555-1570, <https://doi.org/10.5194/acp-19-1555-2019>, 2019.

701 Lin, C., Huang, R.-J., Duan, J., Zhong, H., and Xu, W.: Primary and secondary organic nitrate in
702 northwest China: a case study, *Environ. Sci. Technol. Lett.*, 8, 947-953,
703 <https://doi.org/10.1021/acs.estlett.1c00692>, 2021.

704 Meder, M., Peräkylä, O., Varelas, J. G., Luo, J., Cai, R., Zhang, Y., Kurtén, T., Riva, M., Rissanen, M.,
705 Geiger, F. M., Thomson, R. J., and Ehn, M.: Selective deuteration as a tool for resolving
706 autoxidation mechanisms in α -pinene ozonolysis, *Atmos. Chem. Phys.*, 23, 4373-4390,
707 <https://doi.org/10.5194/egusphere-2022-1131>, 2023.

708 Mentel, T., Springer, M., Ehn, M., Kleist, E., Pullinen, I., Kurtén, T., Rissanen, M., Wahner, A., and Wildt,
709 J.: Formation of highly oxidized multifunctional compounds: autoxidation of peroxy radicals
710 formed in the ozonolysis of alkenes—deduced from structure—product relationships, *Atmos. Chem.*
711 *Phys.*, 15, 6745-6765, <https://doi.org/10.5194/acp-15-6745-2015>, 2015.

712 Molteni, U., Simon, M., Heinritzi, M., Hoyle, C. R., Bernhammer, A.-K., Bianchi, F., Breitenlechner, M.,
713 Brilke, S., Dias, A., Duplissy, J., Frege, C., Gordon, H., Heyn, C., Jokinen, T., Kürten, A., Lehtipalo,
714 K., Makhmutov, V., Petäjä, T., Pieber, S. M., Praplan, A. P., Schobesberger, S., Steiner, G., Stozhkov,
715 Y., Tomé, A., Tröstl, J., Wagner, A. C., Wagner, R., Williamson, C., Yan, C., Baltensperger, U.,
716 Curtius, J., Donahue, N. M., Hansel, A., Kirkby, J., Kulmala, M., Worsnop, D. R., and Dommen, J.:
717 Formation of highly oxygenated organic molecules from α -pinene ozonolysis: chemical
718 characteristics, mechanism, and kinetic model development, *ACS Earth Space Chem.*, 3, 873-883,
719 <https://doi.org/10.1021/acsearthspacechem.9b00035>, 2019.

720 Nozière, B., Kalberer, M., Claeys, M., Allan, J., D'Anna, B., Decesari, S., Finessi, E., Glasius, M., Grgic,
721 I., and Hamilton, J. F.: The molecular identification of organic compounds in the atmosphere: state
722 of the art and challenges, *Chem. Rev.*, 115, 3919-3983, 2015.

723 Orlando, J. J. and Tyndall, G. S.: Laboratory studies of organic peroxy radical chemistry: an overview

724 with emphasis on recent issues of atmospheric significance, *Chem. Soc. Rev.*, 41, 6294-6317,
725 <https://doi.org/10.1039/C2CS35166H>, 2012.

726 Otkjær, R. V., Jakobsen, H. H., Tram, C. M., and Kjaergaard, H. G.: Calculated hydrogen shift rate
727 constants in substituted alkyl peroxy radicals, *J. Phys. Chem. A*, 122, 8665-8673,
728 <https://doi.org/10.1021/acs.jpca.8b06223>, 2018.

729 Pye, H., Chan, A., Barkley, M., and Seinfeld, J.: Global modeling of organic aerosol: the importance of
730 reactive nitrogen (NO_x and NO₃), *Atmos. Chem. Phys.*, 10, 11261-11276,
731 <https://doi.org/10.5194/acp-10-11261-2010>, 2010.

732 Roger, Atkinson, Sara, M., Aschmann, James, N., Pitts, and Jr.: Rate constants for the gas-phase reactions
733 of the OH radical with a series of monoterpenes at 294 ± 1 K, *Int. J. Chem. Kinet.*, 2004.

734 Shen, H., Vereecken, L., Kang, S., Pullinen, I., Fuchs, H., Zhao, D., and Mentel, T. F.: Unexpected
735 significance of a minor reaction pathway in daytime formation of biogenic highly oxygenated
736 organic compounds, *Sci. Adv.*, 8, eabp8702, <https://doi.org/10.1126/sciadv.abp8702>, 2022.

737 Sindelarova, K., Granier, C., Bouarar, I., Guenther, A., Tilmes, S., Stavrou, T., Müller, J.-F., Kuhn, U.,
738 Stefani, P., and Knorr, W.: Global data set of biogenic VOC emissions calculated by the MEGAN
739 model over the last 30 years, *Atmos. Chem. Phys.*, 14, 9317-9341, [https://doi.org/10.5194/acp-14-](https://doi.org/10.5194/acp-14-9317-2014)
740 [9317-2014](https://doi.org/10.5194/acp-14-9317-2014), 2014.

741 Tyndall, G., Cox, R., Granier, C., Lesclaux, R., Moortgat, G., Pilling, M., Ravishankara, A., and
742 Wallington, T.: Atmospheric chemistry of small organic peroxy radicals, *J. Geophys. Res.-Atmos.*,
743 106, 12157-12182, 2001.

744 Villenave, E. and Lesclaux, R.: Kinetics of the cross reactions of CH₃O₂ and C₂H₅O₂ radicals with
745 selected peroxy radicals, *J. Phys. Chem. C*, 100, 14372-14382, <https://doi.org/10.1021/jp960765m>,
746 1996.

747 Wang, Y., Zhao, Y., Li, Z., Li, C., Yan, N., and Xiao, H.: Importance of hydroxyl radical chemistry in
748 isoprene suppression of particle formation from α -pinene ozonolysis, *ACS Earth Space Chem.*, 5,
749 487-499, <https://doi.org/10.1021/acsearthspacechem.0c00294>, 2021.

750 Wolfe, G. M., Marvin, M. R., Roberts, S. J., Travis, K. R., and Liao, J.: The framework for 0-D
751 atmospheric modeling (F0AM) v3. 1, *Geosci. Model Dev.*, 9, 3309-3319,
752 <https://doi.org/10.5194/gmd-9-3309-2016>, 2016.

753 Xu, L., Møller, K. H., Crouse, J. D., Otkjær, R. V., Kjaergaard, H. G., and Wennberg, P. O.:
754 Unimolecular reactions of peroxy radicals formed in the oxidation of α -pinene and β -pinene by
755 hydroxyl radicals, *J. Phys. Chem. A*, 123, 1661-1674, <https://doi.org/10.1021/acs.jpca.8b11726>,
756 2019.

757 Yao, M., Zhao, Y., Hu, M., Huang, D., and Yan, N.: Multiphase reactions between secondary organic
758 aerosol and sulfur dioxide: kinetics and contributions to sulfate formation and aerosol aging,
759 *Environ. Sci. Technol. Lett.*, <https://doi.org/10.1021/acs.estlett.9b00657>, 2019.

760 Zhang, H., Yee, L. D., Lee, B. H., Curtis, M. P., Worton, D. R., Isaacman-VanWertz, G., Offenberg, J. H.,
761 Lewandowski, M., Kleindienst, T. E., and Beaver, M. R.: Monoterpenes are the largest source of
762 summertime organic aerosol in the southeastern United States, *Proc. Natl. Acad. Sci. U. S. A.*, 115,
763 2038-2043, <https://doi.org/10.1073/pnas.1717513115>, 2018.

764 Zhao, Y., Thornton, J. A., and Pye, H. O. T.: Quantitative constraints on autoxidation and dimer formation
765 from direct probing of monoterpene-derived peroxy radical chemistry, *Proc. Natl. Acad. Sci. U. S.*
766 *A.*, 115, 12142-12147, <https://doi.org/10.1073/pnas.1812147115>, 2018.

767 Zhao, Y., Yao, M., Wang, Y. Q., Li, Z. Y., Wang, S. Y., Li, C. X., and Xiao, H. Y.: Acylperoxy Radicals

768 as Key Intermediates in the Formation of Dimeric Compounds in alpha-Pinene Secondary Organic
769 Aerosol, *Environ. Sci. Technol.*, 56, 14249-14261, 10.1021/acs.est.2c02090, 2022.
770 Zhao, Z. X., Zhang, W., Alexander, T., Zhang, X., Martin, D. B. C., and Zhang, H. F.: Isolating a-Pinene
771 Ozonolysis Pathways Reveals New Insights into Peroxy Radical Chemistry and Secondary Organic
772 Aerosol Formation, *Environ. Sci. Technol.*, 55, 6700-6709, 10.1021/acs.est.1c02107, 2021.
773